the FEBS Journal

Binding of non-natural 3′-nucleotides to ribonuclease A

Cara L. Jenkins[1], Nethaji Thiyagarajan[2], Rozamond Y. Sweeney[3], Michael P. Guy[3], Bradley R. Kelemen[3], K. Ravi Acharya[2] and Ronald T. Raines[1,3]

1 Department of Chemistry, University of Wisconsin-Madison, WI, USA
2 Department of Biology and Biochemistry, University of Bath, UK
3 Department of Biochemistry, University of Wisconsin-Madison, WI, USA

Keywords
arabinonucleotide; enzyme inhibitor; 2′-fluoro-2′-deoxynucleotide; ribonuclease; X-ray crystallography

Correspondence
K. R. Acharya, Department of Biology and Biochemistry, University of Bath, Claverton Down, Bath BA2 7AY, UK
Fax: +44 1225 386779
Tel. +44 1225 386238
E-mail: k.r.acharya@bath.ac.uk
R. T. Raines, Department of Biochemistry, University of Wisconsin–Madison, 433 Babcock Drive, Madison, WI 53706-1544, USA
Fax: +1 608 262 3453
Tel: +1 608 262 8588
E-mail: raines@biochem.wisc.edu

(Received 4 October 2004, revised 24 November 2004, accepted 2 December 2004)

doi:10.1111/j.1742-4658.2004.04511.x

2′-Fluoro-2′-deoxyuridine 3′-phosphate (dU^FMP) and arabinouridine 3′-phosphate (araUMP) have non-natural furanose rings. dU^FMP and araUMP were prepared by chemical synthesis and found to have three- to sevenfold higher affinity than uridine 3′-phosphate (3′-UMP) or 2′-deoxyuridine 3′-phosphate (dUMP) for ribonuclease A (RNase A). These differences probably arise (in part) from the phosphoryl groups of 3′-UMP, dU^FMP, and araUMP ($pK_a = 5.9$) being more anionic than that of dUMP ($pK_a = 6.3$). The three-dimensional structures of the crystalline complexes of RNase A with dUMP, dU^FMP and araUMP were determined at < 1.7 Å resolution by X-ray diffraction analysis. In these three structures, the uracil nucleobases and phosphoryl groups bind to the enzyme in a nearly identical position. Unlike 3′-UMP and dU^FMP, dUMP and araUMP bind with their furanose rings in the preferred pucker. In the RNase A·araUMP complex, the 2′-hydroxyl group is exposed to the solvent. All four 3′-nucleotides bind more tightly to wild-type RNase A than to its T45G variant, which lacks the residue that interacts most closely with the uracil nucleobase. These findings illuminate in atomic detail the interaction of RNase A and 3′-nucleotides, and indicate that non-natural furanose rings can serve as the basis for more potent inhibitors of catalysis by RNase A.

Ribonucleases catalyse the cleavage of RNA. These enzymes are abundant in living systems, where they play a variety of roles [1,2]. For example, angiogenin is a homologue of bovine pancreatic ribonuclease (RNase A [3,4]; EC 3.1.27.5) that promotes neovascularization. Angiogenin relies on its ability to cleave RNA for its angiogenic activity [5,6]. An effective inhibitor of the ribonucleolytic activity of angiogenin could diminish its angiogenic activity, which is an effective means to limit tumor growth [7]. Selective ribonuclease inhibitors could also be useful tools in studying the roles of various ribonucleases *in vitro* and *in vivo* [8].

Known nucleotide-based inhibitors of ribonucleases rely on three strategies. Most common are competitive inhibitors that resemble RNA. Shapiro and coworkers have developed especially potent inhibitors of RNase A based on two nucleosides linked by a pyrophosphoryl group [9–11]. Using a different approach, Widlanski and coworkers showed that 3′-(4-(fluoromethyl)phenyl phosphate)uridine is a mechanism-based inactivator of RNase A [12]. Finally, a new strategy has used an *N*-hydroxyurea nucleotide to recruit zinc(II), which then chelates to active-site residues of microbial ribonucleases [13,14]. Each of these strategies

Abbreviations
araUMP, arabinouridine 3′-phosphate; dU^FMP, 2′-fluoro-2′-deoxyuridine 3′-phosphate; 6-FAM, 6-carboxyfluorescein; RNase A, unglycosylated bovine pancreatic ribonuclease; PDB, Protein Data Bank; 6-TAMRA, 6-carboxytetramethylaminorhodamine.

is based on nucleotides containing a ribose or deoxyribose ring. Is that choice optimal?

Here, we report on the inhibition of a ribonuclease by two 3′-nucleotides containing non-natural furanose rings: 2′-fluoro-2′-deoxyuridine 3′-phosphate (dU^FMP) and arabinouridine 3′-phosphate (araUMP). We describe efficient syntheses of these non-natural 3′-nucleotides, determine the pK_a value of their phosphoryl groups, and measure their ability to bind to wild-type RNase A and a variant (T45G RNase A) that lacks the residue responsible for nucleobase recognition. We find that both non-natural 3′-nucleotides have significantly more affinity for wild-type RNase A than do deoxyuridine 3′-phosphate (dUMP) and uridine 3′-phosphate (UMP), two 3′-nucleotides containing natural furanose rings. Finally, we determine the structure of each RNase A·3′-nucleotide complex at high resolution, thereby revealing the basis for the differential inhibition.

Results

Syntheses of 3′-nucleotides

The syntheses of deoxyuridine 3′-phosphate (dUMP, **5a**) and 2′-fluoro-2′-deoxyuridine 3′-phosphate (dU^FMP, **5b**) were accomplished starting from unprotected nucleosides by the route shown in Scheme 1. A synthesis for dUMP had been reported [15], but involves a phosphorylating agent that is not available commercially. dU^FMP had also been synthesized, but its synthesis involves harsh conditions and an involved purification [16]. The advantages of the route in Scheme 1 include the mild conditions and high yield of the phosphorylation step, the use of commercially available reagents, the facile deprotection of the trityl group, and the high purity of the final product after debenzylation.

Briefly, **1** was protected at the 5′-position by treating it with trityl chloride in dry pyridine at reflux to yield **2** [17]. Subsequent phosphorylation at the 3′-position was achieved by reacting **2** with diisopropyl dibenzyl phosphoramidite in the presence of 4,5-dicyanoimidazole followed with oxidation with 3-chloroperoxybenzoic acid to yield **3** [18,19]. Deprotection was achieved in two steps, removing the trityl group first in a mixture of dry trifluoroacetic acid and trifluoroacetic anhydride, followed by addition of methanol to complete the initial deprotection [20]. The resulting dibenzyl phosphate **4** was deprotected by hydrogenolysis using Pd/C as the catalyst to give dUMP (**5a**) and dU^FMP (**5b**) in 51 and 47% overall yield, respectively.

Arabinouridine 3′-monophosphate (araUMP, **10**) was synthesized from uridine by the route shown in Scheme 2. This is a novel route to araUMP from starting materials that are not only available commercially, but also inexpensive. Two other routes to araUMP have been reported. One starts from a 2′,3′-epoxyuridine derivative that is not available commercially [21], and provides a mixture of isomers; the other starts from cytidine 2′,3′-cyclic phosphate [22,23], which is expensive.

Briefly, uridine was protected at the 5′-position by treatment with trityl chloride in pyridine, and then reacted with thiocarbonyldiimidazole to give

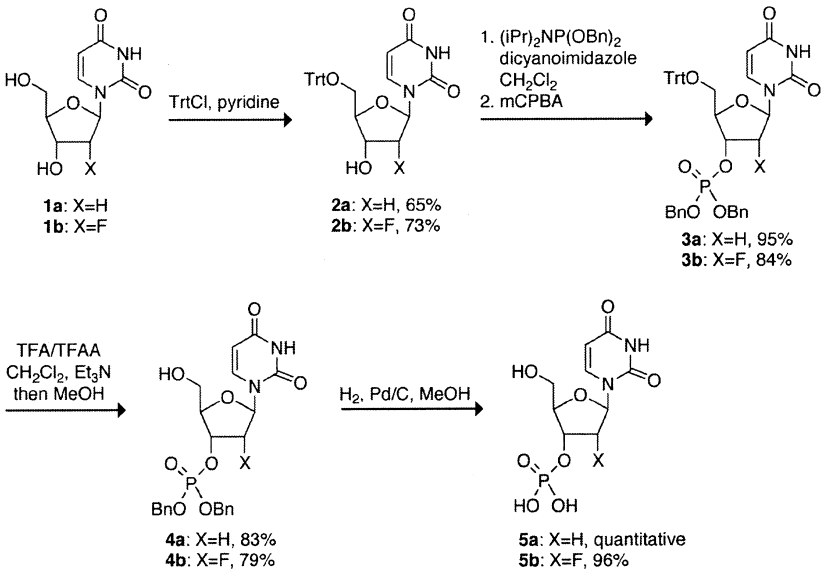

Scheme 1. Synthetic route to dUMP and dU^FMP.

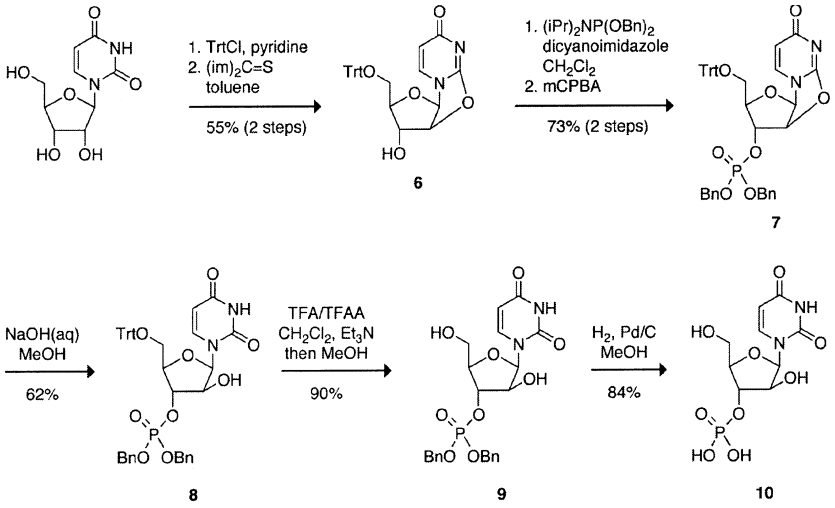

Scheme 2. Synthetic route to araUMP.

5′-trityl-O^2,2′-cyclouridine, **6** [24]. Compound **6** was then phosphorylated at the 3′-position to provide **7** [18,19]. The protected arabinouridine monophosphate **8** was generated by treatment of **7** with one equivalent of aqueous sodium hydroxide in methanol [25], followed by two-step deprotection (*vide supra*) to give araUMP (**10**) in 19% overall yield.

Values of pK_a

The phosphoryl pK_a values of 3′-UMP, dUMP, dU^FMP, and araUMP were measured by using ^{31}P NMR spectroscopy, and are listed in Table 1. The pK_a values of 3′-UMP, araUMP, and dU^FMP are within error of each other, whereas the pK_a value of dUMP is, as expected from a previous report [26], greater than that of the other three. The differences in pK_a values likely arise from through-bond inductive effects. No stereoelectronic component is apparent, as the phosphoryl groups of 3′-UMP and araUMP have the same pK_a values.

Table 1. Values of pK_a and K_i for 3′-nucleotides. Phosphoryl group pK_a values were determined by ^{31}P NMR spectroscopy in 0.10 M buffer. K_i values were determined in Mes/NaOH buffer, pH 6.0, containing NaCl (50 mM).

		K_i (μM)	
Nucleoside 3′-phosphate	pK_a	Wild-type RNase A	T45G RNase A
3′-UMP	5.84 ± 0.05	39 ± 2	89 ± 9
dUMP	6.29 ± 0.07	18 ± 3	≥1700
dU^FMP	5.89 ± 0.10	5.5 ± 0.7	181 ± 15
araUMP	5.85 ± 0.06	6 ± 1	≥1000

Values of K_i

The values of K_i for the four 3′-nucleotides were measured by their ability to inhibit the cleavage of the fluorogenic substrate 6-FAM-dArU$(dA)_2$-TAMRA by wild-type RNase A and its T45G variant [27], and are listed in Table 1. All four 3′-nucleotides were potent inhibitors of the wild-type enzyme, whereas inhibition of T45G RNase A was less pronounced—by up to three orders-of-magnitude. The two non-natural nucleotides, dU^FMP and araUMP, were the most potent inhibitors of wild-type RNase A.

Three-dimensional structures

The three-dimensional structures of the complexes of RNase A with dUMP, dU^FMP and araUMP were determined at high resolution by using X-ray crystallography (Fig. 1; Table 2). The atomic coordinates have been deposited in the Protein Data Bank (PDB; http://www.rcsb.org) with accession codes 1W4P, 1W4Q, and 1W4O, respectively. The structure of the RNase A·3′-UMP complex (PDB entry 1O0N) was reported previously at a resolution of 1.5 Å [28].

The structure of the 3′-nucleotide bound at the active site was clear in all three complexes (except for molecule B in the araUMP complex, due to severe cracking of those crystals while soaking), as observed from the electron density maps (Fig. 2). Protein atoms in structures of the complexes superimpose well with that of free RNase A (PDB entry 1AFU [29]), with a root mean square deviation near 0.52 Å. The interactions made in the dUMP, dU^FMP, and araUMP complexes are similar

Fig. 1. Schematic representation of RNase A in complex with 3′-nucleotides. dUMP (**5a**), dark green; dU^FMP (**5b**), gold; araUMP (**10**), blue.

Table 2. Crystallographic statistics.

RNase A complex	dUMP	araUMP	dU^FMP
Resolution (Å)	50–1.69	50–1.60	50–1.68
Outermost shell (Å)	1.75–1.69	1.66–1.60	1.74–1.68
Reflections measured	184 596	455 952	239 956
Unique reflections	27 984	30 191	27 669
R_{symm}[a]	0.093	0.086	0.047
Outermost shell	0.122	0.517	0.086
Completeness			
Outermost shell (%)	91.4 (94.2)	89.9 (88.5)	94.8 (87.6)
$< I/\sigma I >$ (outermost shell)	9.83	10.3	5.18
R_{cryst}[b]	0.22	0.23	0.21
Outermost shell	0.21	0.50	0.29
R_{free}[c]	0.23	0.25	0.24
Outermost shell	0.27	0.54	0.33
Number of solvent molecules	291	203	310
RMS deviation from ideality			
In bond lengths (Å)	0.010	0.005	0.004
In angles (°)	1.5	1.2	1.3
Average *B* factor (Å^2)	18.4	27.92	14.95

[a] $R_{symm} = \Sigma_h\Sigma_i|I(h) - I_i(h)|/\Sigma_h\Sigma_i I_i(h)$, where $I_i(h)$ and $I(h)$ are the i^{th} and the mean measurements of the intensity of reflection h, respectively.
[b] $R_{cryst} = \Sigma_h||F_o| - |F_c||/\Sigma_h|F_o|$, where F_o and F_c are the observed and calculated structure factors amplitudes of reflection h, respectively.
[c] R_{free} is equal to R_{cryst} for a randomly selected 5% subset of reflections not used in the refinement [45].

(Table 3), as the nucleotides bind predominantly in the P_1, B_1 and P_2 subsites of RNase A [30]. Predominant hydrogen bonds were observed between uracil and Thr45; the 3′-phosphate with the side chains of Gln11, His12, Lys41, and His119 and the main chain of Phe120 at the catalytic site. In all three complexes, the uridine binds in an anti conformation,

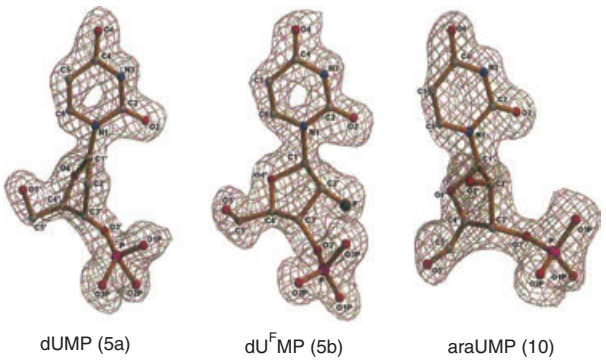

Fig. 2. Portion of the electron density maps ($2F_o–F_c$) of dUMP (**5a**), dU^FMP (**5b**), and araUMP (**10**) in the RNase A·3′-nucleotide complexes.

and its ribose adopts a C_3-*exo*, C_2-*endo*, and O_4-*endo* pucker in dUMP, araUMP, and dU^FMP, respectively [31] (Table 4). The difference in conformation of the ribose moiety can be attributed to the distinct functional groups and stereochemistry at the $C_{2'}$ position (Fig. 3).

Discussion

The results described herein reveal that 3′-nucleotides with a non-natural furanose ring can have a greater affinity for a ribonuclease than do 3′-nucleotides with a ribose or deoxyribose ring. The values of K_i for inhibition of catalysis by RNase A increase in the order: $dU^FMP \approx$ araUMP < dUMP < 3′-UMP (Table 1). The relative affinity of araUMP for wild-type RNase A measured herein is twofold greater than that reported previously [23]. The pK_a of the phosphoryl group contributes to this order, as dianionic 3′-nucleotides are known to be more potent inhibitors of RNase A than monoanionic 3′-nucleotides [9]. The pK_a value of dUMP is 0.4 units greater than that of the other 3′-nucleotides (Table 1). Likewise, the K_i value of dUMP for RNase A is approximately threefold greater than those of dU^FMP and araUMP.

3′-UMP has less affinity for RNase A than would be expected from its pK_a alone. Its weaker binding appears to arise from its 2′-OH group participating in more unfavourable interactions with the enzyme than do the 2′ groups of the other 3′-nucleotides. These unfavourable interactions are probably reinforced by the tight interaction between the uracil base and Thr45 (*vide infra*), and result in the distortion of its ribose ring. The furanose rings of unbound 3′-UMP and dU^FMP reside predominantly in the C_3-*endo* (N) conformation (Fig. 3) [16,32]. Yet in the RNase ·3′-UMP complex, the ribose ring is in

Table 3. Putative hydrogen bonds in the RNase A·3′-nucleotide complexes.

3′-Nucleotide	Atom	RNase A residue	Distance (Å)
dUMP	O_2	Thr45-N	2.82
	N_3	Thr45-$O_{\gamma1}$	2.81
	O_{1P}	His12-$N_{\varepsilon2}$	2.86
	O_{1P}	Phe120-N	3.29
	O_{2P}	Gln11-$N_{\varepsilon2}$	2.87
	O_{3P}	His119-$N_{\delta1}$	2.56
	$O_{3'}$	Lys41-N_{ε}	2.92
	O_4	Water	2.68
	O_4	Water	3.30
	$O_{4'}$	Water	3.08
	O_{2P}	Water	3.22
	O_{3P}	Water	2.79
araUMP	O_2	Thr45-N	2.87
	N_3	Thr45-$O_{\gamma1}$	2.70
	O_{3P}	His12-$N_{\varepsilon2}$	2.69
	O_{3P}	Phe120-N	2.99
	O_{1P}	Gln11-$N_{\varepsilon2}$	2.66
	O_{2P}	His119-$N_{\delta1}$	2.66
	$O_{3'}$	Lys41-N_{ε}	3.10
	O_4	Water	2.57
	O_4	Water	3.33
	$O_{2'}$	Water	2.84
	$O_{4'}$	Water	3.06
	O_{1P}	Water	3.26
	O_{3P}	Water	3.03
dU^FMP	O_2	Thr45-N	2.61
	N_3	Thr45-$O_{\gamma1}$	2.76
	O_{1P}	Gln11-$N_{\varepsilon2}$	2.93
	O_{2P}	His119-$N_{\delta1}$	2.57
	O_{3P}	His12-$N_{\varepsilon2}$	2.79
	O_{3P}	Phe120–N	3.09
	$O_{3'}$	Lys41-N_{ε}	3.45
	O_4	Water	2.75
	O_4	Water	2.91
	O_{1P}	Water	2.78
	O_{2P}	Water	2.92
	O_{3P}	Water	2.95

Table 4. Torsion angles of 3′-nucleotides in the RNase A·3′-nucleotide complexes.

	dUMP	araUMP	dU^FMP
Backbone torsion angles			
$O_{5'}$–$C_{5'}$–$C_{4'}$–$C_{3'}$ (γ)	86.3 (+*sc*)	73.0 (+*sc*)	62.9 (+*sc*)
$C_{5'}$–$C_{4'}$–$C_{3'}$–$O_{3'}$ (δ)	123.4 (+*ac*)	94.8 (+*ac*)	66.7 (+*sc*)
$C_{5'}$–$C_{4'}$–$C_{3'}$–$C_{2'}$	−99.7	−145.7	−158.4
$C_{4'}$–$C_{3'}$–$C_{2'}$–$O_{2'}$	–	93.0	−134.1
Glycosyl torsion angles			
O_4–C_1–N_1–C_2 (χ′)	−107.3 (*anti*)	−156.2 (*anti*)	176.0 (*anti*)
Pseudorotation angles			
$C_{4'}$–$_4$–$C_{1'}$–$C_{2'}$ (ν_0)	2.5	−40.3	−27.9
$O_{4'}$–$C_{1'}$–$C_{2'}$–$C_{3'}$ (ν_1)	23.6	50.9	16.3
$C_{1'}$–$C_{2'}$–$C_{3'}$–$C_{4'}$ (ν_2)	−41.8	−39.3	−2.8
$C_{2'}$–$C_{3'}$–$C_{4'}$–$O_{4'}$ (ν_3)	42.7	17.9	−16.0
$C_{3'}$–$C_{4'}$–$O_{4'}$–$C_{1'}$ (ν_4)	−28.9	15.2	28.8
Phase	201	144	96
	$C_{3'}$-*exo*	$C_{2'}$-*endo*	$O_{4'}$-*endo*
Phosphoryl torsion angles			
$C_{2'}$–$C_{3'}$–$O_{3'}$–P	85.1	89.2	103.5
$C_{4'}$–$C_{3'}$–$O_{3'}$–P (ε)	−147.4 (–*ac*)	−158.4 (+*ap*)	−121.8 (–*ac*)

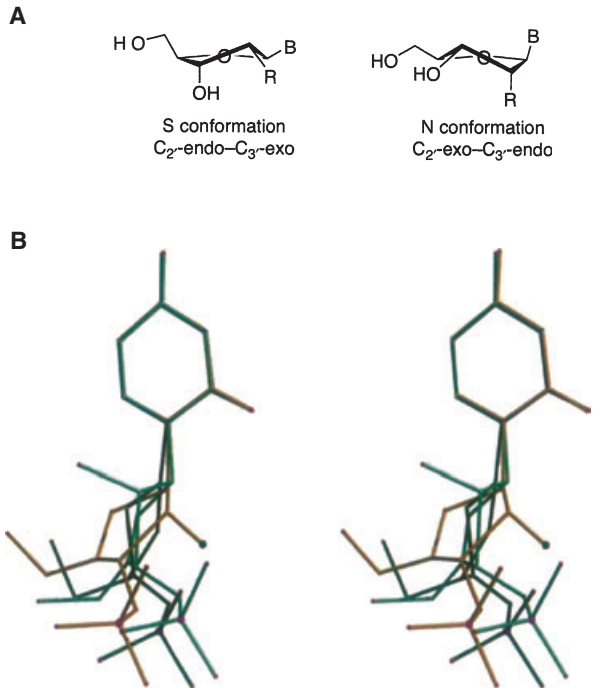

Fig. 3. (A) S and N conformation of nucleosides. R = H favours the S conformation; R = OH,F favours the N conformation. (B) Stereodiagram of 3′-nucleotides in the RNase A·3′-nucleotide complexes, superimposed with respect to their uracil ring. dUMP (**5a**), dark green; dU^FMP (**5b**), gold; araUMP (**10**), blue.

the C_2-*endo* (S) conformation [28]. Similarly, the furanose ring of dU^FMP in the RNase A·dU^FMP complex is in the O_4-*endo* conformation. In contrast, the furanose rings of dUMP and araUMP are not required to take on an unfavourable pucker upon binding to RNase A, as both reside in the $C_{2'}$-*endo* conformation in the complex and free in solution [33–35]. These two 3′-nucleotides have hydrogen in place of the 2′-OH and -F of 3′-UMP and dU^FMP, which could minimize steric conflicts with active-site residues. It is noteworthy that the relative weak affinity of 3′-UMP supports the hypothesis that ground-state destabilization contributes to the catalytic prowess of RNase A [36].

Solvation also appears to affect the affinity of the 3′-nucleotides for RNase A. The 2′-OH group of 3′-UMP must be desolvated upon binding to RNase A

(Fig. 4). In contrast, the 2′-H and -F of dUMP and dU^FMP can form only weak hydrogen bonds with water [37], and the 2′-OH of araUMP is oriented away from the active-site residues and need not be desolvated upon binding to RNase A (Fig. 4).

All four 3′-nucleotides bind more weakly to T45G RNase A than to the wild-type enzyme. This decrease in affinity underlines the importance of the interaction between Thr45 and pyrimidine nucleobases in substrate binding [36,38,39]. Moreover, the relative affinity of the 3′-nucleotides for T45G RNase A follows a much different trend, with the K_i values increasing in the order: 3′-UMP < dU^FMP << araUMP,dUMP (Table 1). The affinity of the 3′-nucleotides for T45G RNase A appears to be sensitive to the pucker of the furanose ring: 3′-UMP and dU^FMP, which prefer the C_3-*endo* conformation [16,32], bind more tightly than do dUMP and araUMP, which prefer the C_2-*endo* conformation [33–35]. Without the presence of Thr45 as an anchor, a 3′-nucleotide can orient its furanose ring and phosphoryl group so as to optimize favourable contacts with active-site residues. For example, 3′-UMP could form a hydrogen bond between its 2′-OH and an active-site residue in T45G RNase A instead of being subjected to the steric constraints that impose an unfavourable ring pucker upon binding to the wild-type enzyme. Such a hydrogen bond could be the source of the twofold higher affinity of T45G RNase A for 3′-UMP than dU^FMP.

Two anchor points appear to dominate the protein–nucleic acid interactions studied herein. The uracil ring and phosphoryl group of dUMP, dU^FMP, and araUMP bind similarly to wild-type RNase A (Table 1; Figs 1 and 4), despite large differences in furanose ring pucker (Fig. 3B). For example, the two most effective inhibitors of catalysis by wild-type RNase A, dU^FMP and araUMP, prefer different puckers in solution but have indistinguishable K_i values. The absence of one of these anchor points in the T45G variant leads to a much broader range in affinity (Table 1).

New applications have emerged for arabinonucleosides. For example, Dharma and coworkers have demonstrated that arabinonucleotides are effective antisense agents [40]. In addition, the antineoplastic drug fludarabine is an arabinonucleoside, and the antineoplastic drug clofarabine is a 2′-fluoro-2′-deoxyarabinonucleoside. We find that araUMP (as well as dU^FMP) binds more tightly to RNase A than do analogous natural 3′-nucleotides. Hence, we put forth araUMP (and dU^FMP) for consideration in the creation of new high-affinity ligands for RNase A and its homologues.

Experimental procedures

General

Reagents obtained from commercial sources were used without further purification. Wild-type RNase A and its T45G variant were prepared by procedures reported previously [38,39,41]. 3′-UMP was obtained from Sigma Chemical (St. Louis, MO). dUMP (**5a**) and dU^FMP (**5b**) were synthesized by the route shown in Scheme 1; araUMP (**10**) was synthesized by the route shown in Scheme 2 (*vide infra*).

Dry dichloromethane was drawn from a Cycletainer from Mallinckrodt Baker (Phillipsburg, NJ). TLC was performed using aluminum-backed plates coated with silica gel

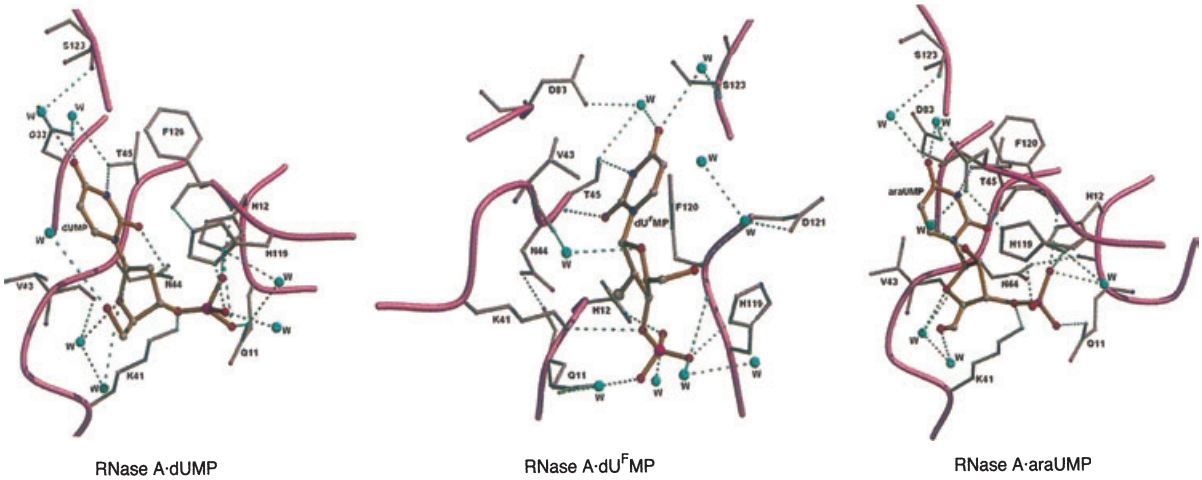

Fig. 4. Details of the active–site interactions in the RNase A·3′-nucleotide complexes. Water molecules are represented by small spheres; hydrogen bonds are indicated by dashed lines.

containing F_{254} phosphor and visualized by UV illumination or staining with I_2, *p*-anisaldehyde or phosphomolybdic acid. NMR spectra were obtained with a Bruker AC-300 (Rheinstetten, Germany) or Varian UNITY-500 (Palo Alto, CA) spectrometer. Mass spectra were obtained with a Micromass LCT electrospray ionization (ESI) instrument (Milford, MA).

5′-Trityl-2′-deoxyuridine (2a)

2′-Deoxyuridine (**1a**; 0.492 g, 2.16 mmol) was placed in a dry, 50-mL round-bottomed flask. Trityl chloride (0.714 g, 2.56 mmol) and pyridine (10 mL) were added, and the reaction mixture was stirred for 48 h at room temperature under Ar(g). The reaction mixture was concentrated under reduced pressure, and the residue was dissolved in dichloromethane and washed once with 1 M HCl and twice with water. The organic layer was dried over $MgSO_4$(s), filtered, and concentrated. The residue was crystallized from ethyl acetate/hexanes to yield **2a** as a white powder (661 mg, 65.0%). ^{1}H NMR (300 MHz, dimethyl sulfoxide-d_6) δ: 7.80 (d, $J = 8.1$ Hz, 1H), 7.22–7.41 (m, 15H), 6.29 (t, $J = 6.3$ Hz, 1H), 5.35 (d, $J = 8.1$ Hz, 1H), 4.54 (dt, $J = 6.1$, 3.9 Hz, 1H), 4.06 (dd, $J = 3.1$, 6.8 Hz, 1H), 3.44 (d, $J = 3.1$ Hz, 2H), 2.18–2.49 (ABMX, $J_{AB} = 13.7$ Hz, $J_{AX} = 6.3$ Hz, $J_{AM} = 4.2$ Hz, $J_{BX} = 6.4$ Hz, $J_{BM} = 0$ Hz, 2H).

5′-Trityl-2′-fluoro-2′-deoxyuridine (2b)

2′-Fluoro-2′-deoxyuridine (**1b**) was synthesized according to the procedure of Maruyama and coworkers [25]. Nucleoside **1b** (3.164 g, 12.85 mmol) was dissolved in dry pyridine (20 mL), and this solution was concentrated to an oil under reduced pressure. The resulting oil was dissolved in dry pyridine (50 mL), and trityl chloride (5.485 g, 19.58 mmol) was added, followed by additional dry pyridine (18 mL). The reaction mixture was heated to reflux under Ar(g) for 4 h, and then concentrated under reduced pressure to a yellow oil. Residual pyridine was removed under reduced pressure as an azeotrope with toluene. The resulting oil was dissolved in dichloromethane and washed once with 1 M HCl, once with saturated $NaHCO_3$(aq), and once with water. The organic layer was dried over $MgSO_4$(s), filtered, and concentrated. The crude product was purified by silica gel chromatography, eluting with MeOH (2.5–5% v/v) in CH_2Cl_2 to yield **2b** as a white solid (4.587 g, 73.1%). ^{1}H NMR (300 MHz, $CDCl_3$ + CD_3OD) δ: 7.95 (d, $J = 8.4$ Hz, 1H), 7.42–7.24 (m, 15H), 6.04 (dd, $J = 16.5$, 1.2 Hz, 1H), 5.28 (d, $J = 8.1$ Hz, 1H), 4.98 (ddd, $J = 52.2$, 4.3, 1.0 Hz, 1H), 4.53 (ddd, $J = 22.2$, 8.7, 4.2 Hz, 1H), 4.13 (bd, $J = 8.4$ Hz, 1H), 3.58 (m, 2H). ^{13}C NMR (75.4 MHz, $CDCl_3$ + CD_3OD) δ: 163.93, 150.12, 142.91, 139.95, 128.42, 127.73, 127.14, 101.92, 93.58 (d, $J = 188.0$ Hz), 87.75 (d, $J = 34.6$ Hz), 87.29, 81.53, 68.01 (d, $J = 16.7$ Hz), 60.93. ^{19}F NMR (282.1 MHz, $CDCl_3$ + CD_3OD) δ: −201.44 (ddd, $J = 52.2$, 22.0, 16.9 Hz). ESI–MS (M + Na): 511.1651 (observed), 511.1645 (calculated).

5′-Trityl-2′-deoxyuridine 3′-dibenzylphosphate (3a)

Dicyanoimidazole (127 mg, 1.08 mmol) was suspended in dry dichloromethane (25 mL) in an oven-dried 100-mL round-bottomed flask containing a stir bar. Diisopropyldibenzylphosphoramidite (220 μL, 0.98 mmol) was added to the suspension at room temperature, and the mixture was allowed to stir for 01.25 h. 5′-Trityl-2′-deoxyuridine (175 mg, 0.37 mmol) suspended in dry CH_2Cl_2 (10 mL) was added, and the reaction mixture was stirred at room temperature for an additional 01.25 h. The reaction mixture was then cooled to 0 °C, and solid *m*-chloroperoxybenzoic acid (351 mg) was added in one portion. The reaction mixture was stirred at 0 °C for 15 min, the ice bath was removed, and the reaction mixture was stirred at room temperature for an additional 1 h. The reaction mixture was poured into a separation funnel containing ethyl acetate and washed three times with $Na_2S_2O_5$(aq) (10% w/v), three times with saturated $NaHCO_3$(aq) (75 mL total), twice with 1 M HCl (50 mL total), once with water, and once with saturated NaCl(aq). The organic layer was then dried over $MgSO_4$(s), filtered, and concentrated under reduced pressure. The resulting solid was purified by silica gel chromatography, eluting with MeOH (2.5% v/v) in CH_2Cl_2 to yield **3a** as a white solid (256 mg, 94.7%). ^{1}H NMR (300 MHz, $CDCl_3$) δ: 9.80 (bs, 1H), 7.63 (d, $J = 8.4$ Hz, 1H), 7.34–7.25 (m, 25H), 6.30 (dd, $J = 7.8$, 6.3 Hz, 1H), 5.31 (dd, $J = 8.4$, 1.8 Hz, 1H), 5.09–4.98 (m, 5H), 4.18 (m, 1H), 3.34 (m, 1H), 2.49 (ddd, $J = 13.8$, 5.7, 2.1 Hz, 1H), 2.24–2.15 (m, 1H). ^{13}C NMR (75.4 MHz, $CDCl_3$) δ: 163.36, 150.22, 142.84, 139.68, 135.27 (d, $J = 6.0$ Hz), 128.64 (d, $J = 2.0$ Hz), 128.55 (d, $J = 1.8$ Hz), 128.51, 128.00 (d, $J = 2.6$ Hz), 127.38, 87.61, 84.45, 84.32 (d, $J = 6.0$ Hz), 77.57 (d, $J = 5.2$ Hz), 69.62 (t, $J = 5.6$ Hz), 62.94, 39.20. ^{31}P NMR (121.4 MHz, $CDCl_3$, ^{1}H decoupled) δ: −1.40. ESI–MS (M + Na): 753.2338 (observed), 753.2342 (calculated).

5′-Trityl-2′-fluoro-2′-deoxyuridine 3′-dibenzylphosphate (3b)

The preparation of **3b** was carried out in a manner similar to that used for the preparation of **3a**. The product was purified by silica gel chromatography, eluting with MeOH (2.5–5% v/v) in CH_2Cl_2 to yield **3b** as a white solid (4.623 g, 84.1%). ^{1}H NMR (300 MHz, $CDCl_3$) δ: 9.71 (s, 1H), 7.77 (d, $J = 8.1$ Hz, 1H), 7.38–7.21 (m, 25H), 6.07 (d, $J = 16.2$ Hz, 1H), 5.25 (d, $J = 8.4$ Hz, 1H), 5.20–4.87 (m, 6H), 4.23 (bd, $J = 7.2$ Hz, 1H), 3.54 (m, 2H). ^{13}C NMR (75.4 MHz, $CDCl_3$) δ: 163.11, 149.85, 142.76, 139.52, 135.14 (dd, $J = 6.8$, 6.6 Hz), 128.64, 128.53, 128.01, 127.85, 127.45, 102.57, 91.44 (d, $J = 193.6$ Hz), 87.80 (d, $J = 33.6$ Hz),

87.75, 80.42 (d, $J = 8.7$ Hz), 71.96 (dd, $J = 16.1$, 4.4 Hz), 69.86 (dd, $J = 7.0$, 6.5 Hz), 60.61. ^{19}F NMR (282.1 Hz, $CDCl_3$) δ: −200.03 (ddd, $J = 52.2$, 16.5, 14.2 Hz). ^{31}P NMR (121.4 MHz, $CDCl_3$, ^{1}H decoupled) δ: −1.50. ESI–MS (M + Na): 771.2230 (observed), 771.2248 (calculated).

2′-Deoxyuridine 3′-dibenzylphosphate (4a)

Compound **3a** (270 mg, 0.36 mmol) was dissolved in dry CH_2Cl_2 (5 mL) under Ar(g), and a solution of trifluoroacetic acid (139 μL, 1.8 mmol) and trifluoroacetic anhydride (255 μL, 1.8 mmol) in dry CH_2Cl_2 (0.6 mL) was added by syringe at room temperature. The reaction mixture, which turned bright yellow, was stirred at room temperature for 10 min, cooled to 0 °C, and then stirred for an additional 10 min. Upon addition of triethylamine (250 μL, 1.79 mmol), the bright yellow colour disappeared. After 5 min, MeOH (10 mL) was added, the reaction mixture was stirred for an additional 5 min, and then concentrated under reduced pressure. The residue was dissolved in CH_2Cl_2, and washed once with 1 M NaCl. The organic layer was dried over $MgSO_4$(s), filtered, and concentrated under reduced pressure. The resulting product was purified by silica gel chromatography, eluting with MeOH (5% v/v) in CH_2Cl_2 to yield **4a** as a white solid (151 mg, 82.6%). ^{1}H NMR (300 MHz, $CDCl_3$) δ: 8.48 (bs, 1H), 7.61 (d, $J = 7.8$, 1H), 7.38–7.34 (m, 10H), 6.08 (dd, $J = 7.5$, 6.0 Hz, 1H), 5.72 (dd, $J = 8.1$, 2.1 Hz, 1H), 5.12–5.02 (m, 4H), 4.99–4.92 (m, 1H), 4.06 (m, 1H), 3.81–3.67 (m, 2H), 2.67 (bt, 1H), 2.40–2.21 (m, 2H). ^{13}C NMR (75.4 MHz, $CDCl_3$) δ: 163.73, 150.38, 140.70, 135.17 (d, $J = 6.7$ Hz), 128.76, 128.61, 128.02, 102.54, 85.75, 77.93, 69.78 (dd, $J = 3.2$, 5.7 Hz), 61.64, 38.72. ^{31}P NMR (121.4 MHz, $CDCl_3$, ^{1}H decoupled) δ: −1.38. ESI–MS (M + Na): 511.1241 (observed), 511.1246 (calculated).

2′-Fluoro-2′-deoxyuridine 3′-dibenzylphosphate (4b)

The preparation of **4b** was carried out in a similar manner to that used for the preparation of **4a**. The crude product was purified by silica gel chromatography, eluting with MeOH (2.5–5% v/v) in CH_2Cl_2 to yield **4b** as a white solid (1.601 g, 78.6%). ^{1}H NMR (300 MHz, $CDCl_3$ + CD_3OD) δ: 7.88 (d, $J = 8.1$ Hz, 1H), 7.38–7.32 (m, 10H), 6.01 (dd, $J = 2.7$, 15.3 Hz, 1H), 5.73 (d, $J = 8.4$ Hz, 1H), 5.13–4.85 (m, 6H), 4.14 (m, 1H), 3.78 (m, 2H). ^{13}C NMR (75.4 MHz, $CDCl_3$ + CD_3OD) δ: 163.86, 150.19, 140.31, 134.82 (dd, $J = 6.5$, 5.8 Hz), 128.69, 128.46, 127.89 (d, $J = 5.7$ Hz), 102.41, 90.94 (d, $J = 195.1$ Hz), 87.62 (d, $J = 33.8$ Hz), 82.40 (d, $J = 6.3$ Hz), 72.43 (dd, $J = 14.7$, 4.4 Hz), 70.02 (d, $J = 5.8$ Hz), 59.21. ^{19}F NMR (282.13 MHz, $CDCl_3$ + CD_3OD) δ: −202.10 (ddd, $J = 52.2$, 16.5, 14.0). ^{31}P NMR (121.4 MHz, $CDCl_3$ + CD_3OD, ^{1}H decoupled) δ: −1.55. ESI–MS (M + Na): 529.1171 (observed), 529.1152 (calculated).

2′-Deoxyuridine 3′-phosphate (dUMP, 5a)

2′-Deoxyuridine 3′-dibenzylphosphate (177 mg, 0.36 mmol) was placed in a 100-mL round-bottomed flask, which was then flushed with Ar(g) for 5 min. Palladium on carbon (16 mg) was added, and the flask was flushed again with Ar(g) for 5 min. A 4 : 1 solution of MeOH and NH_4HCO_3(aq) (1% w/v) was added slowly. H_2(g) was introduced via a balloon. The reaction mixture was stirred under H_2(g) for 4 h, and then filtered through a Celite plug, concentrated under reduced pressure to dryness, and placed under vacuum overnight to yield **5a** as a colourless solid (133 mg, 100%). ^{1}H NMR (300 MHz, D_2O) δ: 7.86 (d, $J = 8.1$ Hz, 1H), 6.29 (t, $J = 6.7$ Hz, 1H), 5.87 (d, $J = 8.4$ Hz, 1H), 4.71 (septet, $J = 3.6$ Hz, 1H), 4.17 (m, 1H), 3.87–3.74 (m, 2H), 2.59–2.33 (m, 2H). ^{13}C NMR (75.4 MHz, D_2O) δ 167.12, 152.53, 143.05, 103.29, 88.10 (d, $J = 5.7$ Hz), 86.56. 75.83 (d, $J = 4.0$ Hz), 62.25, 39.08. ^{31}P NMR (121.4 MHz, D_2O, ^{1}H decoupled) δ: −0.13. ESI–MS (M–H): 307.0342 (observed), 307.0331 (calculated).

2′-Fluoro-2′-deoxyuridine 3′-phosphate (dU^FMP, 5b)

The preparation of **5b** was performed in a manner similar to that for the preparation of **5a**, to yield **5b** as a colourless solid. (1.010 g, 95.7%). ^{1}H NMR (300 MHz, D_2O) δ: 7.66 (d, $J = 8.1$ Hz, 1H), 5.79 (d, $J = 18.9$ Hz, 1H), 5.64 (d, $J = 8.1$ Hz, 1H), 5.04 (dd, $J = 52.2$, 4.3 Hz, 1H), 4.34 (dtd, $J = 22.5$, 9.0, 4.2 Hz, 1H), 3.94 (m, 1H), 3.71 (m, 2H). ^{13}C NMR (75.4 MHz, D_2O) δ: 167.14, 152.15, 143.68, 103.17, 92.78 (d, $J = 190.3$ Hz), 90.71 (d, $J = 35.5$ Hz), 83.21 (d, $J = 7.8$ Hz), 71.82 (d, $J = 14.8$ Hz), 60.64. ^{19}F NMR (282.13 MHz, D_2O) δ: −199.02 (ddd, $J = 52.2$, 19.3, 17.4 Hz). ^{31}P NMR (121.4 MHz, D_2O, ^{1}H decoupled) δ: −0.37. ESI–MS (M–H): 325.0221 (observed), 325.0237 (calculated).

5′-Trityluridine

Uridine (5.040 g, 20.6 mmol) and freshly distilled pyridine (45 mL) were combined in a dry 200-mL round-bottomed flask, and cooled to 0 °C under Ar(g). Trityl chloride (5.770 g, 20.7 mmol) in pyridine (25 mL) was added via syringe. The reaction mixture was allowed to warm to room temperature and stirred for 4 days. Ethyl acetate was added to the reaction mixture, which was then transferred to a separation funnel. The organic layer was washed twice with 2 M HCl, once with saturated $NaHCO_3$(aq), and then once with saturated NaCl(aq). The organic layer was dried over $MgSO_4$(s), filtered, and concentrated under reduced pressure.

The resulting residue was crystallized from EtOAc/hexanes to yield 5′-trityluridine as a white solid (6.076 g, 61% yield.) ^{1}H NMR (300 MHz, CD_3OD + $CDCl_3$) δ: 7.97 (d, J = 8.1 Hz, 1H), 7.23–7.45 (m, 15H), 5.89 (d, J = 3.3 Hz, 1H), 5.26 (d, J = 8.1 Hz, 1H), 4.42 (dd, J = 6.1, 5.2 Hz, 1H), 4.24 (dd, J = 5.0, 3.3 Hz, 1H), 4.13 (dt, J = 5.9, 2.8 Hz, 1H), 3.49 (ABX, J_{AB} = 11.0 Hz, J_{AX} = 3.0 Hz, J_{BX} = 2.5 Hz, 2H). ^{13}C NMR (75.4 MHz, DMSO) δ: 163.04, 150.50, 143.42, 140.62, 128.31, 128.02, 127.20, 101.48, 88.95, 86.42, 82.34, 73.40, 69.53, 63.25. ESI–MS (M + Na): 509.1677 (observed), 509.1689 (calculated).

5′-Trityl-O^2,2′-cyclouridine (6)

5′-Trityluridine (10.692 g, 22.1 mmol) and 1,1′-thiocarbonyldiimidazole (5.087 g, 28.5 mmol) were combined in a 250-mL round-bottomed flask. Toluene (120 mL) was added, and the reaction mixture was heated to reflux for 1 h. The reaction mixture was then allowed to cool to room temperature. The tan solid product was removed by filtration, washed with MeOH, and recrystallized from MeOH to yield **6** as an off-white solid (9.247 g, 89.7%). ^{1}H NMR (300 MHz, DMSO-d_6) δ: 7.94 (d, J = 7.4 Hz, 1H), 7.19–7.32 (m, 15H), 6.33 (d, J = 5.5 Hz, 1H), 5.99 (d, J = 4.6 Hz, 1H), 5.86 (d, J = 7.5 Hz, 1H), 5.21 (d, J = 6.4 Hz,1H), 4.24 (m, 1H), 4.06 (m, 1H), 2.89 (m, 2H). ^{13}C NMR (75.4 MHz, DMSO) δ: 170.88, 159.25, 143.30, 136.66, 128.02, 127.94, 127.08, 108.88, 89.70, 88.44, 86.64, 85.96, 74.73, 63.01. ESI–MS (M + Na): 491.1578 (observed), 491.1583 (calculated).

5′-Trityl-O^2,2′-cyclouridine 3′-dibenzylphosphate (7)

The preparation of **7** was carried out in a manner similar to that used for the preparation of **3a**. The product was purified by silica gel chromatography, eluting with MeOH (5% v/v) in CH_2Cl_2 to yield **7** as a white solid (3.417 g, 72.7%). ^{1}H NMR (300 MHz, $CDCl_3$) δ: 7.32–7.23 (m, 25H), 7.16 (d, J = 7.2 Hz, 1H), 6.03 (d, J = 5.4 Hz, 1H), 5.87 (d, J = 7.5 Hz, 1H), 5.11–4.92 (m, 6H), 4.51 (dd, J = 7.2, 6.9 Hz, 1H), 2.85 (m, 2H). ^{13}C NMR (75.4 MHz, $CDCl_3$) δ: 171.07, 158.66, 142.81, 134.90 (d, J = 5.5 Hz), 134.10, 128.91 (d, J = 3.5 Hz), 128.69 (d, J = 3.0 Hz), 128.22, 127.94, 127.35, 110.34, 89.91, 87.11, 86.18 (d, J = 6.3 Hz), 85.62 (d, J = 4.5 Hz), 79.73 (d, J = 5.4 Hz), 70.16 (d, J = 5.9 Hz), 62.01. ^{31}P NMR (121.4 MHz, $CDCl_3$, ^{1}H decoupled) δ: −1.95. ESI–MS (M + Na): 751.2151 (observed), 751.2185 (calculated).

5′-Trityl-arabinouridine 3′-dibenzylphosphate (8)

Methanol (40 mL) was added to **7** (2.983 g, 4.09 mmol) in a 100-mL round bottomed flask. The solid dissolved at first and then precipitated, so CH_2Cl_2 was added until the solution was clear again. Aqueous NaOH (1 M; 4 mL, 4 mmol) was added dropwise via a Pasteur pipette, and the reaction mixture was stirred at room temperature for 8 h. The bulk of the solvent was evaporated under reduced pressure. The residue was dissolved in dichloromethane, and the resulting solution was washed with water. (The pH of the water wash was ≈13) Glacial acetic acid (0.5 mL) was added, the layers were separated, and the organic layer was washed again with water. The layers were separated, and the organic layer was washed twice with saturated $NaHCO_3$(aq) and twice with saturated NaCl(aq). The organic layer was dried over $MgSO_4$(s), filtered, and concentrated under reduced pressure. The crude product was purified by silica gel chromatography, eluting with EtOAc/CH_2Cl_2 (1 : 1, v/v) to yield **8** as a white solid (1.888 g, 61.8%).

^{1}H NMR (300 MHz, $CDCl_3$) δ: 10.02 (bs, 1H), 7.59 (d, J = 8.1 Hz, 1H), 7.41–7.17 (m, 25H), 6.15 (d, J = 4.8 Hz, 1H), 5.35 (d, J = 8.1 Hz, 1H), 4.98–4.89 (m, 5H), 4.81 (m, 1H), 4.55 (m, 1H), 4.03 (m, 1H), 3.40 (m, 2H). ^{13}C NMR (75.4 MHz, $CDCl_3$) δ: 164.05, 150.56, 143.19, 141.94, 135.15 (d, J = 6.1 Hz), 128.63, 128.53, 128.03 (d, J = 2.8 Hz), 127.90, 127.23, 100.99, 87.25, 85.24, 81.05 (d, J = 5.9 Hz), 80.94 (d, J = 9.8 Hz), 74.50, 69.86 (d, J = 5.4 Hz), 62.03. ^{31}P NMR (121.4 MHz, $CDCl_3$, ^{1}H decoupled) δ: −1.17. ESI–MS (M + Na): 769.2303 (observed), 769.2291 (calculated).

Arabinouridine 3′-dibenzylphosphate (9)

The preparation of **9** was carried out in a manner similar to that used for the preparation of **4a**. The crude product was purified by silica gel chromatography, eluting with MeOH (5% v/v) in CH_2Cl_2 to yield **9** as a light yellow solid (1.084 g, 89.6%). ^{1}H NMR (300 MHz, $CDCl_3$) δ: 10.33 (bs, 1H), 7.70 (d, J = 8.4 Hz, 1H), 7.34–7.26 (m, 10H), 6.04 (d, J = 3.9 Hz, 1H), 5.60 (d, J = 8.4 Hz, 1H), 5.44 (d, J = 6.3 Hz, 1H), 5.05–4.98 (m, 4H), 4.82 (m, 1H), 4.52 (m, 1H), 4.46 (m, 1H), 4.03 (m, 1H), 3.76 (m, 2H). ^{13}C NMR (75.4 MHz, $CDCl_3$) δ: 164.59, 150.47, 142.19, 135.02 (d, J = 6.0 Hz), 128.74, 128.58, 128.04 (d, J = 2.8 Hz), 100.72, 86.02, 83.21, 81.44 (d, J = 4.1 Hz), 73.98 (d, J = 4.0 Hz), 70.00 (dd, J = 5.4, 4.8 Hz), 60.98. ^{31}P NMR (121.4 MHz, $CDCl_3$, ^{1}H decoupled) δ: −1.60. ESI–MS (M + Na): 527.1180 (observed), 527.1195 (calculated).

Arabinouridine 3′-phosphate (araUMP, 10)

The preparation of **10** was carried out in a manner similar to that used for the preparation of **5a**. The product was purified by reverse-phase HPLC with elution by the gradient: 0–10 min, 95% A, 5% B; 10–20 min, 95–50% A, 5–50% B; 20–25 min, 50–95% A, 50–5% B. Buffer A was H_2O containing trifluoroacetic acid (0.1% v/v); Buffer B was CH_3CN containing trifluoroacetic acid (0.1% v/v). The

desired product eluted between 6 and 8 min, and the byproduct eluted at 21 min. The fractions were combined and evaporated under reduced pressure to yield **10** as a colourless solid (558 mg, 83.8%). ^{1}H NMR (300 MHz, D_2O) δ: 7.67 (d, $J = 8.1$ Hz, 1H), 5.98 (d, $J = 4.2$ Hz, 1H), 5.67 (d, $J = 8.1$ Hz, 1H), 4.41–4.35 (m, 2H), 4.03 (m, 1H), 3.72 (m, 2H). ^{13}C NMR (125.7 MHz, D_2O) δ: 167.14, 152.18, 144.08, 101.88, 86.73, 84.16 (d, $J = 4.9$ Hz), 80.51 (broad), 75.18 (d, $J = 4.9$ Hz), 61.55. ^{31}P NMR (121.4 MHz, D_2O, ^{1}H decoupled) δ: −0.37. ESI–MS (M–H): 323.0272 (observed), 323.0280 (calculated).

Determination of phosphoryl-group pK_a values

The pK_a of the phosphoryl group of each 3′-nucleotide was determined by using ^{31}P NMR spectroscopy. A 3′-nucleotide was dissolved in D_2O (1.0 mL) to make a 100 mM stock solution. An aliquot (100 μL) of the stock solution was added to 0.10 M buffer (900 μL), and the resulting solution was filtered. The buffers used were oxalic acid (p$K_a = 1.3$), citric acid (3.1 and 4.8), succinic acid (4.2), Mes (6.15), Mops (7.2), Tris (8.3), CHES (9.5), and CAPS (10.4), each adjusted to a pH near its pK_a with 2 M HCl or 2 M NaOH. A filtered sample (900 μL) was placed in an NMR tube, and its ^{31}P NMR chemical shift was measured with a Bruker DMX-400 MHz (wide bore) spectrometer equipped with a quattro-nucleus probe or a Bruker DMX-500 MHz spectrometer equipped with a broadband probe, referenced to an external standard of H_3PO_4, and ^{1}H-decoupled. The pH of each sample was measured with a Beckman Ω40 pH meter. Data were fitted to Eqn (1) with the program DELTAGRAPH 4.0 (Red Rock Software; Salt Lake City, UT).

$$\delta = \frac{\delta_{low} + \delta_{high} \times 10^{(pH - pK_a)}}{1 + 10^{pH - pK_a}} \quad (1)$$

The reported values are the mean (± SE) of two determinations.

Determination of K_i values

The K_i value for each 3′-nucleotide was determined from its ability to inhibit the cleavage of 6-FAM-dArU(dA)$_2$-6-TAMRA by RNase A [27]. Fluorescence emission intensity was measured at 515 nm, with excitation at 493 nm. Each assay was carried out in 2.0 mL of 20 mM Mes/NaOH buffer, pH 6.0, containing NaCl (50 mM), RNase A (wild-type, 0.5 pM; T45G, 12.5 pM), and 6-FAM-dArU(dA)$_2$-6-TAMRA (0.06 μM). The value of $\Delta F/\Delta t$ was measured for 3 min after the addition of RNase A. An aliquot (0.5 μL) of a dilute solution of 3′-nucleotide (2 mM) dissolved in water was added, and $\Delta F/\Delta t$ was measured for 3 min in the presence of the 3′-nucleotide. Additional aliquots of 3′-nucleotide were added at 3-min intervals, doubling the volume of the aliquot with each addition until an 8-μL aliquot had been added. Then, an aliquot (4 μL) of a concentrated solution of 3′-nucleotide (10 mM) was added, and subsequent additions again doubled in volume until a 32-μL aliquot had been added, for a total of nine additions (75.5 μL) altogether. In each assay, 15% of the substrate was cleaved. The loss of fluorescence intensity was corrected for dilution by using the data from an assay in which buffer instead of 3′-nucleotide was added to the enzymatic reaction. The K_i values were determined by fitting the data to Eqn (2) with the program DELTAGRAPH 4.0.

$$\Delta F/\Delta t = (\Delta F/\Delta t)_0 \left(\frac{K_i}{K_i + [I]} \right) \quad (2)$$

In Eqn (2) $(\Delta F/\Delta t)_0$ is the ribonucleolytic activity prior to the addition of the 3′-nucleotide.

During the assays, the fluorescence intensity was quenched at high concentrations of 3′-nucleotide. To correct for this quenching, the following assay was conducted. To 2.0 mL of 20 mM Mes–NaOH buffer, pH 6.0, containing NaCl (50 mM) was added 1 μL of the substrate 6-FAM–dArU(dA)$_2$–6-TAMRA (60 μM), followed 3 min later by 2 μL of a concentrated solution of wild-type RNase A (1.5 mM). At 3-min intervals thereafter, aliquots (5, 10, 20, and 40 μL) of a dilute solution of araUMP (1.72 mM) were added to the same cuvette, and the fluorescence intensity was measured. In a separate assay, aliquots (5, 10, 20, and 40 μL) of a concentrated solution of araUMP (25.7 mM) were added, and the fluorescence intensity was measured. The two data sets were corrected for loss of fluorescence intensity due to dilution, and then combined and fitted to Eqn (3) using DELTAGRAPH 4.0. A quenching correction factor for each point was calculated using Eqn (3) (where F_∞ is the value of the final fluorescence intensity measurement and $k = -30.77$) and the 3′-nucleotide concentration in the cuvette. Each value of $\Delta F/\Delta t$ was divided by the correction factor to give the corrected value. The correction factor was the same for all the 3′-nucleotides, assuming that the fluorescence quenching arises from the uracil moiety of the 3′-nucleotide.

$$y = (1 - F_\infty)e^{kx} + F_\infty \quad (3)$$

X-ray crystallography

Crystals of RNase A (Sigma Chemical) were grown using the vapour diffusion technique as described previously [29]; they belong to the space group C2, with two molecules per asymmetric unit. Crystals of the 3′-nucleotide complexes were obtained by soaking the RNase A crystals in 20 mM sodium citrate buffer, pH 5.5, containing PEG 4000 (25% w/v) and dUMP (50 mM), araUMP (1 mM), or dU^{F}MP (12.5 mM) for 45, 60, and 75 min, respectively, prior to data collection. Diffraction data for the three complexes were collected at 100 K (the reservoir buffer with 30% PEG 4000 was used as cryoprotectant) on stations PX 14.1 and

PX 9.6 from a single crystal at the Synchrotron Radiation Source (Daresbury, UK) using an ADSC Quantum 4 CCD detector. All diffraction images were integrated using HKL2000 [42]. Phases were obtained by using the structure of free RNase A [29] as a starting model. The refinement was carried out with the CNS suite [43] and the model building was carried out with O [44]. Initial model building and refinement was carried out without the 3′-nucleotide. In each data set, a set of reflections were kept aside for the calculation of R_{free} [45]. The 3′-nucleotide and water molecules were modelled using the $2F_o–F_c$ and $F_o–F_c$ SIGMAA weighted maps. The topology and parameter files for the 3′-nucleotides were either generated manually and/or using the Hic-up server [46] http://alpha2.bmc.uu.se/hicup/. All three structures have good geometry, and the ϕ and ψ angles of > 87% of the protein residues are in the most favorable region of a Ramachandran plot. All structural diagrams were prepared with the program BOBSCRIPT [47].

Acknowledgements

We are grateful to K. E. Hauschild for help with the preparation of wild-type RNase A and its T45G variant, and B. D. Smith and K. A. Dickson for contributive discussions. We thank the staff at the SRS (Daresbury, UK) and S. Iyer for their help during X-ray data collection. This work was supported by Program Grant 067288 (Wellcome Trust, UK) to K.R.A. and grant CA73808 (NIH) to R.T.R. C.L.J. was supported by Chemistry-Biology Interface Training Grant GM08506 (NIH). N.T. was supported by a Post-Graduate studentship from the University of Bath. NMR spectra were obtained at the Magnetic Resonance Facility in the Department of Chemistry at the University of Wisconsin-Madison, which was supported by grants CHE-8813550, CHE-9208463, and CHE-9629688 (NSF), and S10 RR04981-01 and S10 RR08389-01 (NIH).

References

1 Beintema JJ & Kleineidam RG (1998) The ribonuclease A superfamily: General discussion. *Cell Mol Life Sci* **54**, 825–842.
2 D'Alessio G & Riordan JF (1997) Ribonucleases: Structures and Functions. Academic Press, New York.
3 Cuchillo CM, Vilanova M & Nogués MV (1997) Pancreatic ribonucleases. In *Ribonucleases: Structures and Functions* (D'Alessio, G & Riordan, JF, eds), pp. 271–304. Academic Press, New York.
4 Raines RT (1998) Ribonuclease A. *Chem Rev* **98**, 1045–1065.
5 Shapiro R, Fox EA & Riordan JF (1989) Role of lysines in human angiogenin: Chemical modification and site-directed mutagenesis. *Biochemistry* **28**, 1726–1732.
6 Shapiro R & Vallee BL (1989) Site-directed mutagenesis of histidine-13 and histidine-114 of human angiogenin. Alanine derivatives inhibit angiogenin-induced angiogenesis. *Biochemistry* **28**, 7401–7408.
7 Olson KA, Fett JW, French TC, Key ME & Vallee BL (1995) Angiogenin antagonists prevent tumor growth in vivo. *Proc Natl Acad Sci USA* **92**, 442–446.
8 Leonidas DD, Shapiro R, Irons LI, Russo N & Acharya KR (1999) Toward rational design of ribonuclease inhibitors: High resolution crystal structure of a ribonuclease A complex with a potent 3′,5′-pyrophosphate-linked dinucleotide inhibitor. *Biochemistry* **38**, 10287–10297.
9 Russo A, Acharya KR & Shapiro R (2001) Small molecule inhibitors of RNase A and related enzymes. *Methods Enzymol* **341**, 629–648.
10 Russo N & Shapiro R (1999) Potent inhibition of mammalian ribonucleases by 3′,5′-pyrophosphate-linked nucleotides. *J Biol Chem* **274**, 14902–14908.
11 Russo N, Shapiro R & Vallee BL (1997) 5′-Diphosphoadenosine 3′-phosphate is a potent inhibitor of bovine pancreatic ribonuclease A. *Biochem Biophys Res Commun* **231**, 671–674.
12 Stowell JK, Widlanski TS, Kutateladze TG & Raines RT (1995) Mechanism-based inactivation of ribonuclease A. *J Org Chem* **60**, 6930–6936.
13 Higgin JJ, Yakovlev GI, Mitkevich VA, Makarov AA & Raines RT (2003) Zinc-mediated inhibition of a ribonuclease by an N-hydroxyurea nucleotide. *Bioorg Med Chem Lett* **13**, 409–412.
14 Makarov AA, Yakovlev GI, Mitkevich VA, Higgin JJ & Raines RT (2004) Zinc (II) -Mediated inhibition of ribonuclease Sa by an *N*-hydroxyurea nucleotide and its basis. *Biochem Biophys Res Commun* **319**, 152–156.
15 Taktakishvili M & Nair V (2000) A new method for the phosphorylation of nucleosides. *Tetrahedron Lett* **41**, 7173–7176.
16 Antonov IV, Dudkin SM, Karpeiskii MY & Yakovlev GI (1976) The conformations of phosphorylating derivatives of 2′-fluoro-2′-deoxyuridine in solution. *Sov J Bioorg Chem* **2**, 863–872.
17 Codington JF, Doerr IL & Fox JJ (1964) Nucleosides. XVIII. Synthesis of 2′-fluorothymidine, 2′-fluorodeoxyuridine, and other 2′-halogeno-2′-deoxynucleosides. *J Org Chem* **29**, 558–564.
18 Perich JW & Johns RB (1987) A new, convenient and efficient general procedure for the conversion of alcohols into their dibenzyl phosphorotriesters using *N*,*N*-diethyl dibenzyl phosphoramidite. *Tetrahedron Lett* **28**, 101–102.
19 Giner J-L & Ferris WV Jr (2002) Synthesis of 2-C-methyl-D-erythritol-2,4-cyclopyrophosphate. *Org Lett* **4**, 1225–1226.

20 Krainer E & Naider F (1993) A new method for the detritylation of alcohols bearing other reducible and acid-hydrolyzable functionalities. *Tetrahedron Lett* **34**, 1713–1716.
21 Roussev CD, Simeonov MF & Petkov DD (1997) Arabinonucleotide synthesis by the epoxide route. *J Org Chem* **62**, 5238–5240.
22 Nagyvary J (1969) Arabinonucleotides. II. The synthesis of O2,2′-anhydrocytidine 3′-phosphate, a precursor of 1-β-D-arabinosylcytosine. *J Am Chem Soc* **91**, 5409–5410.
23 Pollard DR & Nagyvary J (1973) Inhibition of pancreatic ribonuclease A by arabinonucleotides. *Biochemistry* **12**, 1063–1066.
24 Fox JJ & Wempen I (1965) Nucleosides XXVI. A facile synthesis of 2,2′-anhydro-arabino pyrimidine nucleosides. *Tetrahedron Lett* **6**, 643–646.
25 Sato Y, Utsumi K, Maruyama T, Kimura T, Yamamoto I & Richman DD (1994) Synthesis and hypnotic and anti-human immunodeficiency virus-1 activities of N^3-substituted 2′-deoxy-2′-fluorouridines. *Chem Pharm Bull* **42**, 595–598.
26 Walz FG Jr (1971) Kinetic and equilibrium studies on the interaction of ribonuclease A and 2′-deoxyuridine-3′phosphate. *Biochemistry* **10**, 2156–2162.
27 Kelemen BR, Klink TA, Behlke MA, Eubanks SR, Leland PA & Raines RT (1999) Hypersensitive substrate for ribonucleases. *Nucleic Acids Res* **27**, 3696–3701.
28 Leonidas DD, Chavali GB, Oikonomakos NG, Chrysina ED, Kosmopoulou MN, Vlassi M, Frankling C & Acharya KR (2003) High resolution crystal structures of ribonuclease A complexed with adenylic and uridylic nucleotide inhibitors. Implications for structure-based design of ribonucleolytic inhibitors. *Protein Sci* **12**, 2559–2574.
29 Leonidas DD, Shapiro R, Irons LI, Russo N & Acharya KR (1997) Crystal structures of ribonuclease A complexes with 5′-diphosphoadenosine 3′-phosphate and 5′-diphosphoadenosine 2′-phosphate at 1.7 Å resolution. *Biochemistry* **36**, 5578–5588.
30 Nogués MV, Moussaoui M, Boix E, Vilanova M, Ribó M & Cuchillo CM (1998) The contribution of noncatalytic phosphate-binding subsites to the mechanism of bovine pancreatic ribonuclease A. *Cell Mol Life Sci* **54**, 766–774.
31 Altona C & Sundaralingam M (1972) Conformational analysis of the sugar ring in nucleosides and nucleotides. A new description using the concept of pseudorotation. *J Am Chem Soc* **94**, 8205–8212.
32 Davies DB & Danyluk SS (1975) Nuclear magnetic resonance studies of 2′- and 3′-ribonucleotide structures in solution. *Biochemistry* **14**, 543–554.
33 Guschlbauer W & Jankowski K (1980) Nucleoside conformation is determined by the electronegativity of the sugar substituent. *Nucleic Acids Res* **8**, 1421–1433.
34 Chwang AK & Sundaralingam M (1973) Intramolecular hydrogen bonding in 1-β-D-arabinofuranosylcytosine (Ara-C). *Nat New Biol* **243**, 78–79.
35 Venkateswarlu D & Ferguson DM (1999) Effects of C2′-substitution on arabinonucleic acid structure and conformation. *J Am Chem Soc* **121**, 5609–5610.
36 Kelemen BR, Schultz LW, Sweeney RY & Raines RT (2000) Excavating an active site: The nucleobase specificity of ribonuclease A. *Biochemistry* **39**, 14487–14494.
37 Howard JAK, Hoy VJ, O'Hagan D & Smith GT (1996) How good is fluorine as a hydrogen bond acceptor?. *Tetrahedron* **52**, 12613–12622.
38 delCardayré SB & Raines RT (1994) Structural determinants of enzymatic processivity. *Biochemistry* **33**, 6031–6037.
39 delCardayré SB & Raines RT (1995) A residue to residue hydrogen bond mediates the nucleotide specificity of ribonuclease A. *J Mol Biol* **252**, 328–336.
40 Dahma MJ, Noronha AM, Wilds CJ, Trempe JF, Denisov A, Pon RT & Gehring K (2001) Properties of arabinonucleic acids (ANA & 2′F-ANA): Implications for the design of antisense therapeutics that invoke RNase H cleavage of RNA *Nucleosides Nucleotides Nucleic Acids* **20**, 429–440.
41 delCardayré SB, Ribó M, Yokel EM, Quirk DJ, Rutter WJ & Raines RT (1995) Engineering ribonuclease A: Production, purification, and characterization of wild-type enzyme and mutants at Gln11. *Protein Eng* **8**, 261–273.
42 Otwinowski Z & Minor W (1997) Processing of X-ray diffraction data collected in oscillation mode. *Methods Enzymol* **276**, 307–326.
43 Brunger AT, Adams PD, Clore GM, DeLano WL, Gros P, Grosse-Kunstleve RW, Jiang JS, Kuszewski J, Nilges M, Pannu NS, Read RJ, Rice LM, Simonson T & Warren GL (1998) Crystallography & NMR system: A new software suite for macromolecular structure determination. *Acta Crystallogr D* **54**, 905–921.
44 Jones TA, Zou JY, Cowan SW & Kjeldgaard M (1991) Improved methods for building models in electron density maps and the location of errors in these models. *Acta Crystallogr A* **47**, 110–119.
45 Brunger AT (1992) Free R value: A novel statistical quantity for assessing the accuracy of crystal structures. *Nature* **355**, 472–475.
46 Kleywegt GJ & Jones TA (1998) Databases in protein crystallography. *Acta Crystallogr D* **54**, 1119–1131.
47 Esnouf RM (1997) An extensively modified version of MolScript that includes greatly enhanced coloring capabilities. *J Mol Graph Model* **15**, 132–134.